AGU PUBLICATIONS

Global Biogeochemical Cycles

RESEARCH ARTICLE
10.1002/2013GB004790

Key Points:
- Oxygen deficient zones are a source of N_2O to the South Atlantic mesopelagic
- Nitrifier denitrification produces shallow N_2O in the South Atlantic
- Low-O_2 water along the African continental shelf coincides with N_2O maxima

Supporting Information:
- Readme
- Figure S1
- Figure S2
- Figure S3

Correspondence to:
C. H. Frame,
cframe@post.harvard.edu

Citation:
Frame, C. H., E. Deal, C. D. Nevison, and K. L. Casciotti (2014), N_2O production in the eastern South Atlantic: Analysis of N_2O stable isotopic and concentration data, *Global Biogeochem. Cycles*, *28*, doi:10.1002/2013GB004790.

Received 7 DEC 2013
Accepted 4 OCT 2014
Accepted article online 7 OCT 2014

N_2O production in the eastern South Atlantic: Analysis of N_2O stable isotopic and concentration data

Caitlin H. Frame[1], Eric Deal[2], Cynthia D. Nevison[3], and Karen L. Casciotti[4]

[1]Department of Environmental Sciences, University of Basel, Basel, Switzerland, [2]Institut des Sciences de la Terre, Université Joseph Fourier, Grenoble, France, [3]Institute of Arctic and Alpine Research, University of Colorado Boulder, Boulder, Colorado, USA, [4]Department of Environmental Earth System Science, Stanford University, Palo Alto, California, USA

Abstract The stable isotopic composition of dissolved nitrous oxide (N_2O) is a tracer for the production, transport, and consumption of this greenhouse gas in the ocean. Here we present dissolved N_2O concentration and isotope data from the South Atlantic Ocean, spanning from the western side of the mid-Atlantic Ridge to the upwelling zone off the southern African coast. In the eastern South Atlantic, shallow N_2O production by nitrifier denitrification contributed a flux of isotopically depleted N_2O to the atmosphere. Along the African coast, N_2O fluxes to the atmosphere of up to 46 μmol/m^2/d were calculated using satellite-derived QuikSCAT wind speed data, while fluxes at the offshore stations averaged 0.04 μmol/m^2/d. Comparison of the isotopic composition of the deeper N_2O in the South Atlantic (800 m to 1000 m) to measurements made in other regions suggests that water advected from one or more of the major oxygen deficient zones contributed N_2O to the mesopelagic South Atlantic via the Southern Ocean. This deeper N_2O was isotopically and isotopomerically enriched ($\delta^{15}N^{bulk} - N_2O = 8.7 \pm 0.1$‰, $\delta^{18}O - N_2O = 46.5 \pm 0.2$‰, and Site Preference = 18.7 ± 0.6‰) relative to the shallow N_2O source, indicating that N_2O consumption by denitrification influenced its isotopic composition. The N_2O concentration maximum was observed between 200 m and 400 m and reached 49 nM near the Angolan coast. The depths of the N_2O concentration maximum coincided with those of sedimentary particle resuspension along the coast. The isotopic composition of this N_2O ($\delta^{15}N^{bulk} - N_2O = 5.8 \pm 0.1$‰, $\delta^{18}O - N_2O = 39.7 \pm 0.1$‰, and Site Preference = 9.8 ± 1.0‰) was consistent with production by diffusion-limited nitrate (NO_3^-) reduction to nitrite (NO_2^-), followed by NO_2^- reduction to N_2O by denitrification and/or nitrifier denitrification, with additional N_2O production by NH_2OH decomposition during NH_3 oxidation. The sediment surface, benthic boundary layer, or particles resuspended from the sediments are likely to have provided the physical and chemical conditions necessary to produce this N_2O.

1. Introduction

Nitrous oxide (N_2O) is a greenhouse gas whose production is tied to both the nitrogen cycle and climate conditions [*Davidson et al.*, 2004, 2008]. Rising atmospheric N_2O concentrations over the past 150 to 200 years [*Machida et al.*, 1995; *Battle et al.*, 1996] have been linked to expanding agricultural use of nitrogenous fertilizers [*Nevison and Holland*, 1997; *Holland et al.*, 2005; *Davidson*, 2009]. N_2O emissions to the atmosphere have increased an estimated 40% to 50% over preindustrial levels [*Hirsch et al.*, 2006], while the rate of loss through photochemical reactions in the stratosphere has increased only slightly [*Prather*, 1998]. Most anthropogenic and natural N_2O emissions are the result of microbial conversions of fixed nitrogen in soil as well as marine and other aquatic environments, with a smaller contribution from biomass burning and fossil fuel combustion [*Denman et al.*, 2007].

Variations in atmospheric N_2O concentrations were relatively small in the 12,000 years preceding the industrial era. However, over longer time horizons, large and rapid increases in atmospheric N_2O that are comparable in scale to the present one have accompanied climate transitions between glacial periods and warmer interglacial conditions [*Fluckiger et al.*, 1999, 2002, 2004]. The drivers of these concentration changes are not well understood and proposed mechanisms involve both terrestrial and marine N_2O sources [*Fluckiger et al.*, 2002; *Sowers et al.*, 2003; *Jaccard and Galbraith*, 2011]. The ocean is a net source and reservoir of atmospheric N_2O, containing roughly 65% of the amount of N_2O in the atmosphere [*Houghton et al.*, 1991]

and may influence the rise and fall of atmospheric N_2O concentrations over geological timescales [*Schmittner and Galbraith*, 2008]. Furthermore, factors that affect the volume of low-oxygen (O_2) water associated with oxygen deficient zones (ODZs), such as surface temperatures, mesopelagic ventilation rates, and rates of organic matter sinking and decomposition, may also affect future marine N_2O distributions and emissions [*Keeling et al*., 2010; *Deutsch et al*., 2011].

The largest source of marine N_2O is thought to be nitrification, a form of chemoautotrophy that occurs as ammonium (NH_4^+) is released during organic matter decomposition. Nitrification is the aerobic, two-step oxidation of ammonia (NH_3) to nitrite (NO_2^-) and then nitrate (NO_3^-). These steps are catalyzed by two different groups of microorganisms, namely, ammonia oxidizers and nitrite oxidizers. Observations that cultures and enrichments of ammonia-oxidizing bacteria and archaea produce N_2O [*Goreau et al*., 1980; *Santoro et al*., 2011; *Löscher et al*., 2012] and widely observed correlations between subsurface N_2O, apparent oxygen utilization, and NO_3^- concentrations in the open ocean [*Yoshinari*, 1976; *Cohen and Gordon*, 1978] have led to the conclusion that ammonia oxidizers are the main source of marine N_2O. Ammonia-oxidizing bacteria produce N_2O through the decomposition of hydroxylamine (NH_2OH), an intermediate during NH_3 oxidation to NO_2^-, and also through an enzyme-mediated process known as nitrifier denitrification, which reduces NO_2^- to N_2O [*Hooper and Terry*, 1979; *Poth and Focht*, 1985].

Another potential source of marine N_2O is denitrification, a form of heterotrophy that couples organic matter oxidation with NO_3^- reduction to dinitrogen (N_2) in anoxic or low-O_2 environments. N_2O is an intermediate in the sequential enzymatic reduction of NO_3^- to N_2 during denitrification and may be released as well as consumed by denitrifying cells at rates that depend upon O_2 concentrations and other growth conditions [*Firestone et al*., 1980; *Hochstein et al*., 1984; *McKenney et al*., 1994]. Evidence suggests that active water column denitrification is restricted to stably anoxic regions, also known as ODZs, found in the Eastern Tropical North Pacific (ETNP) and South Pacific (ETSP) and the Arabian Sea. In these regions, local N_2O maxima occur in the oxyclines on the edges of the ODZs, while minima occur in the ODZs themselves [*Cohen and Gordon*, 1978; *Elkins et al*., 1978]. The cycling of N_2O in these regions is complex [*Codispoti and Christensen*, 1985] and may influence N_2O distributions in the broader ocean. Stable isotopic analyses of N_2O can be used to distinguish the sources and cycling of N_2O in these regions and track their influence on N_2O distributions on broader spatial scales.

The isotopic composition of N_2O reflects that of the substrates used to produce it, as well as the isotopic fractionation of molecules that contain different isotopes of N (^{14}N and ^{15}N) and O (^{16}O, ^{17}O, and ^{18}O) during reactions that produce or consume the N_2O. In the ocean, the stable isotopic composition of N_2O provides evidence of how the N_2O was produced and whether it was subsequently subject to partial consumption by denitrification in the water column. Recent laboratory experiments have also closed a number of gaps in our knowledge of the isotopic signatures of the N_2O produced and consumed by microbial processes [*Sutka et al*., 2006; *Ostrom et al*., 2007; *Frame and Casciotti*, 2010; *Santoro et al*., 2011], bringing within reach a more fully resolved understanding of the biological dynamics that influence marine N_2O distributions. Stable isotope systematics have been used to characterize local production and consumption mechanisms influencing dissolved N_2O in marine environments [*Yoshida et al*., 1989; *Ostrom et al*., 2000; *Popp et al*., 2002; *Westley et al*., 2006; *Yamagishi et al*., 2007]. However, sparse spatial and temporal coverage of available marine N_2O isotope data has made it difficult to assess how widespread these processes are in the ocean.

To date, isotopic measurements made on marine N_2O have focused heavily on the Pacific Ocean, particularly the tropical and subtropical gyres [*Kim and Craig*, 1990; *Ostrom et al*., 2000; *Popp et al*., 2002] and the ETNP [*Yoshinari et al*., 1997; *Yamagishi et al*., 2007; *Fujii et al*., 2013] and ETSP [*Charpentier et al*., 2007]. Measurements have also been made in the Arabian Sea [*Yoshinari et al*., 1997; *Naqvi et al*., 1998; *McIlvin and Casciotti*, 2010] and the oxycline of the Black Sea [*Westley et al*., 2006]. Many of these regions are hot spots of marine N_2O production and consumption, but may not be representative of other ocean environments, where dissolved N_2O typically accumulates during the aerobic remineralization of organic matter [*Cohen and Gordon*, 1979] and is eventually released to the atmosphere through vertical mixing and air-sea gas exchange.

Coastal upwelling areas are important sources of N_2O to the atmosphere (e.g., the northwest Indian Ocean [*Law and Owens*, 1990] and northeast Pacific coast [*Lueker et al*., 2003; *Nevison et al*., 2004]). They support large N_2O fluxes because intense vertical mixing draws N_2O-rich deep water to the surface [*Nevison et al*.,

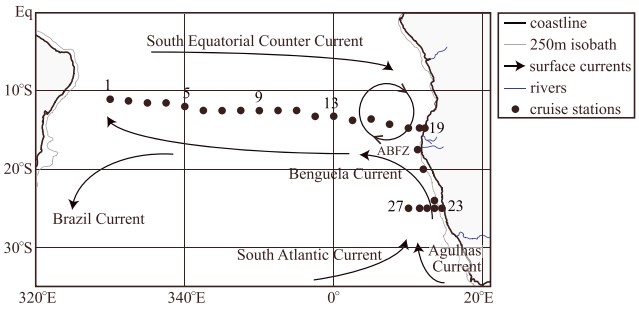

Figure 1. The three legs of the CoFeMUG cruise crossed the South Atlantic, went down the coast of Africa, and then back out to sea. N_2O concentration and isotopic data were collected at stations 5 through 27. ABFZ = the Angola-Benguela Frontal Zone.

1995; *Lueker et al*., 2003; *Charpentier et al*., 2010], and injection of high-nutrient deep water into the mixed layer stimulates primary production and nutrient remineralization processes that enhance local N_2O production [*Lueker et al*., 2003]. The highly productive Benguela upwelling system off the southwestern coast of Africa is a documented source of N_2O to the atmosphere [*Nevison et al*., 2004; *Gutknecht et al*., 2013b] that may become larger as O_2 depletion in this region intensifies [*Stramma et al*., 2008]. Here we report new measurements of the concentration and isotopic composition of dissolved N_2O collected from within this upwelling system as well as the open ocean of the South Atlantic Basin from which we infer the regional and microbial sources of N_2O emitted to the atmosphere.

2. Materials and Methods

Samples were collected during the CoFeMUG cruise, which crossed the South Atlantic during a period of high upwelling between mid-November and mid-December 2007 [*Noble et al*., 2012]. It consisted of three transects (Figure 1): a zonal transect from the coast of Brazil to the Angolan coast (stations 1 to 19, 330°W, 11°S to 12.2°E, 14.75°S), a longitudinal transect along the coasts of Angola and Namibia (stations 19 to 23, 12.2°E, 14.75°S to 14.5°E, 25°S), and a southern zonal transect extending offshore from the coast of Namibia (stations 23 to 27, 14.5°E, 25°S to 10°E, 25°S).

The ship's conductivity-temperature-depth sensors recorded salinity, potential temperature, fluorescence, dissolved O_2, and transmissometer beam attenuation. O_2 sensor data were calibrated with Winkler titrations at the beginning and end of the cruise. Phosphate (PO_4^{3-}), NO_3^-, NO_2^-, NH_4^+, and silicate concentration measurements were made on filtered samples that were kept frozen until analysis. Nutrient concentration measurements were made for all depths and all stations by a nutrient analysis facility (see *Noble et al*. [2012] for details).

Single water samples for N_2O analyses were collected from depths between 10 m and 1000 m at stations 5 through 27. Immediately after rosette recovery, water samples were collected by twice overfilling 160 mL glass serum bottles (Wheaton product no. 223748) from the bottom using Tygon tubing attached to each Niskin bottle. A small headspace was introduced into each sample by pipetting 1 mL of water off the top. It was then poisoned with 100 μL of saturated $HgCl_2$ solution and sealed with a gray butyl septum (MicroLiter Analytics product no. 20-0025) and aluminum crimp. Poisoned samples were stored for approximately 2 months in the dark at room temperature before analysis.

Isotopic analyses of N_2O were made using a Finnigan DELTA^{PLUS} XP isotope ratio mass spectrometer with five collectors (m/z 30, 31, 44, 45, and 46) calibrated according to *Frame and Casciotti* [2010] for isotopomer-specific measurements using a reference N_2O gas calibrated by S. Toyoda ($\delta^{15}N^{bulk} - N_2O = 0.31‰$, $\delta^{18}O - N_2O = 40.85‰$, Site Preference or SP = −1.2‰). Isotopic values are reported on Vienna SMOW and AIR (atmospheric N_2) reference scales. Bottles were purged with He and N_2O was trapped on line with a custom-built purge and trap system [*McIlvin and Casciotti*, 2010]. The molar amount of N_2O contained in each bottle was calculated using a constant linear relationship between N_2O molar quantity and m/z 44 peak area, and then converted to a concentration by dividing this by the volume of seawater extracted (154 mL). Details about measurement precision are discussed at length in *McIlvin and Casciotti* [2010]. Briefly, for triplicate measurements of 160 mL

water samples containing 2.2 nmol of our standard N_2O gas, the standard deviations were 0.09‰ for $\delta^{15}N^{bulk}-N_2O$, 0.25‰ for $\delta^{18}O-N_2O$, 0.33‰ for SP, with m/z 44 peak areas of 4.7 ± 0.04 Vs. Standard deviations were similar for water samples containing 4.5 nmol or 9.0 nmol of standard N_2O. Reported data have been corrected for linear changes in 31/30, 45/44, and 46/44 detector responses with increasing m/z 44 peak areas. All N_2O concentration and isotopic data presented in this paper have been deposited in the Biological and Chemical Oceanography Data Management Office under the CoFeMUG program (http://bcodmo.org/). Contour plots of each transect were made in Igor Pro version 6.03 using linear interpolation between data points.

For calculations of ocean-atmosphere N_2O fluxes, the depth of the mixed layer (MLD) at each station was estimated as the shallowest depth that was within ±0.03 kg/m^3 of the potential density at the reference depth of 10 m [*De Boyer Montégut et al*., 2004]. At coastal stations, a 3 m reference depth was used rather than 10 m in order to avoid using a reference depth within the pycnocline. QuikSCAT wind velocity components were downloaded for the cruise region for each of the 60 days prior to the dates of N_2O sampling and used to calculate the gas transfer velocity (k_{gasex}, units = m/s) of N_2O according to the empirical relationship of *Wanninkhof* [1992],

$$k_{gasex} = 0.31U_{10}^2(Sc/660)^{-0.5}$$

where U_{10} is the wind speed 10 m above the ocean surface (units = m/s) derived from QuikSCAT scatterometer satellite data [e.g., *Bourassa et al*., 2003]. Schmidt numbers (*Sc*) were calculated for the observed sea surface temperatures using the kinematic viscosity formulation of *Sverdrup et al*. [1942] and the molecular diffusivity of N_2O given by *Versteeg and Van Swaaij* [1988]. The impact of daily wind speed variations over the 60 days prior to sample collection was incorporated using the weighting technique of *Reuer et al*. [2007].

At each station, N_2O saturation disequilibrium (ΔN_2O, units = μmol/m^3) in the mixed layer was calculated as the difference between the observed N_2O concentration and the atmospheric equilibrium N_2O concentration calculated using the solubility coefficients of *Weiss and Price* [1980] and assuming a 319 ppb atmospheric mole fraction. Average values of ΔN_2O are reported at stations where there was more than one N_2O measurement in the mixed layer. N_2O fluxes (F_{atm}, units = mol/m^2/s) at each station were calculated as the product of k_{gasex} and ΔN_2O:

$$F_{atm} = k_{gasex}\,\Delta N_2O$$

Flux calculations and parameters used to make them are listed for each station in Table 1. At stations 19, 22, and 23 there were no observations in the mixed layer, so fluxes were not calculated there.

Wind stress curl, which is balanced by ocean upwelling or downwelling (Ekman suction and pumping), was estimated over the 4 weeks corresponding to the cruise by calculating the curl of the directional wind stress components τ_u and τ_v (units = kg/m/s^2) derived from the QuikSCAT wind velocity components *u* and *v* (m/s) [*Milliff and Morzel*, 2001]:

$$\tau_u = \rho_{air}C_DU_{10}u$$
$$\tau_v = \rho_{air}C_DU_{10}v,$$

where the density of air (ρ_{air}) is taken as 1.23 kg/m^3 and C_D is a dimensionless drag coefficient calculated according to *Large et al*. [1994]. Negative values of wind stress curl are favorable to upwelling [*Milliff and Morzel*, 2001].

The rate of coastal upwelling was estimated using alongshore wind stress estimations ($\tau_{alongshore}$, units = kg/m/s^2) from the wind velocity components and coastline coordinates available in NOAA's National Geophysical Data Center database and then translated to a flux of deep water (*M*, units = m^2/s) and volume rate of upwelling (*V*, units = m^3/s) at each latitude along the coast:

$$\tau_{alongshore} = \rho_{air}C_DU_{10}u_{alongshore},$$
$$M = -\tau_{alongshore}/(\rho_{water}f)$$
$$V = -\tau_{alongshore}/(\rho_{water}f)\,dL$$

where *f* is the Coriolis parameter (units = 1/s) and d*L* is a unit length of coastline between the pairs of latitude grid points in the QuikSCAT data set. *V* was calculated for each d*L* between 10°S and 27.5°S for each of the 60 days prior to the sampling dates. The average upwelling velocity (m/s) was calculated by dividing *M* by the Rossby radius of deformation at each latitude for each day during the cruise.

Table 1. Daily N_2O Fluxes Calculated at Each Station and the Parameters Used to Calculate Them

Station	Location (°S,°E)	k_{gasex} (m/d)	Mixed Layer Depth (m)	N_2O Measurement Depth (m)	ΔN_2O (μmol/m^3)	n	ΔN_2O Standard Deviation	Surface Flux, F_{atm} (μmol/m^2/d)
5	12, 340	5.26	59	19, 39	0.4	2	0.06	2.0
6	12.5, 342.5	5.35	20	20	0.2	1	-	1.0
7	12.5, 345	5.41	23	20	0.5	1	-	2.8
8	12.5, 347.5	4.85	49	19, 40	−0.1	2	0.03	−0.3
9	12.5, 350	4.85	44.5	20, 39	0.0	2	0.01	0.0
10	12.5, 352.5	4.77	28	20	0.2	1	-	0.9
11	12.5, 355	4.41	38.5	20	−0.4	1	-	−1.8
12	13.25, 357.5	4.30	47	20	−0.3	1	-	−1.5
13	13.25, 0	4.40	30	20	−0.4	1	-	−1.7
14	13.75, 2.5	3.91	39	20	−0.2	1	-	−0.8
15	13.6, 5	3.86	43	20, 40	3.7	2	5.27	14.1
16	14.25, 7.5	3.66	36	20	0.0	1	-	−0.2
17	14.75, 10	4.86	23	20	5.8	1	-	28.4
18	14.75, 11.5	2.91	18	17	15.6	1	-	45.6
19	14.75, 12.2	3.47	11	-	-	0	-	-
20	17.5, 11.25	4.97	18	11	8.7	1	-	43.4
21	20, 12	3.88	17	10	4.1	1	-	16.1
22	24, 13.5	2.36	11	-	-	0	-	-
23	25, 14.5	2.10	10	-	-	0	-	-
24	25, 13.5	1.97	11	10	1.8	1	-	3.6
25	25, 12.5	2.70	13	10	−0.1	1	-	−0.2
26	25, 11.5	2.25	13	10	0.1	1	-	0.3
27	25, 10	2.47	15	10	0.0	1	-	−0.1

3. Results and Discussion

3.1. Overview

Two neighboring systems of ocean currents and wind patterns interact in the Benguela upwelling zone [*Hutchings et al.*, 2009] (Figure 1). To the south, the Benguela Current flows northward along the coasts of South Africa and Namibia and then moves offshore, causing coastal upwelling between 17°S and 30°S. To the north, a cyclonic gyre draws the Angola Current southward along the continental shelf until it encounters the Benguela Current at the Angola-Benguela Frontal Zone (ABFZ) between 15°S and 17°S. The cruise's northern zonal transect passed through the Angolan subsystem (stations 15 through 19) and ended at the Angolan coast, just north of the ABFZ. The coastal transect (stations 19 through 23) crossed the ABFZ between stations 19 and 20, and encountered strong coastal upwelling at stations 20 and 21 (Figure 2). The ABFZ was marked in the top 300 m by a sharp north-to-south increase in O_2 concentrations (Figure 3a) and a drop in N_2O concentrations (Figure 3b) as older, more nutrient-rich subequatorial South Atlantic Central Water (SACW) flowing southward encountered more recently ventilated subtropical SACW flowing northward [*Gordon and Bosley*, 1991; *Brea et al.*, 2004]. Upwelling rates dropped off again at the latitude of the southern zonal transect (25°S, Figure 2) which was located north of the intense Luderitz upwelling cell [*Hutchings et al.*, 2009].

Minima in $\delta^{15}N^{bulk}$–N_2O, $\delta^{18}O$–N_2O, and SP were observed within 200 m of the surface in both the northern and southern transects and were generally located above the concentration maximum. These minima were most intense at stations 18 and 19 (at 17 m at station 18, $\delta^{15}N^{bulk} - N_2O = 3.4 \pm 0.1‰$, $\delta^{18}O - N_2O = 42.0 \pm 0.2‰$, SP = 5.3 ± 0.6‰ and at 150 m at station 19, $\delta^{15}N^{bulk} - N_2O = 5.2 \pm 0.1‰$, $\delta^{18}O - N_2O = 37.5 \pm 0.2‰$, SP = 6.2 ± 0.6‰) (Figures 3c–3e). These easternmost stations of the northern transect were located in a region where negative wind stress curl drives shallow upwelling [*Chapman and Shannon*, 1987] (Figure 4a) that may have transported subsurface N_2O into the mixed layer and contributed to surface oversaturations of N_2O (positive ΔN_2O) and elevated N_2O fluxes observed at these stations (Figures 4b and 4c and Table 1), even though the wind speed, and therefore the gas transfer velocities, were generally lower in this region than they were to the west (Figure 4d). The wind regime also enhanced surface primary productivity, as suggested by the higher fluorescence maxima at these stations (Figure 4e), and this may have also contributed to surface N_2O oversaturations by stimulating the nutrient cycling processes that sustain NH_3 oxidation.

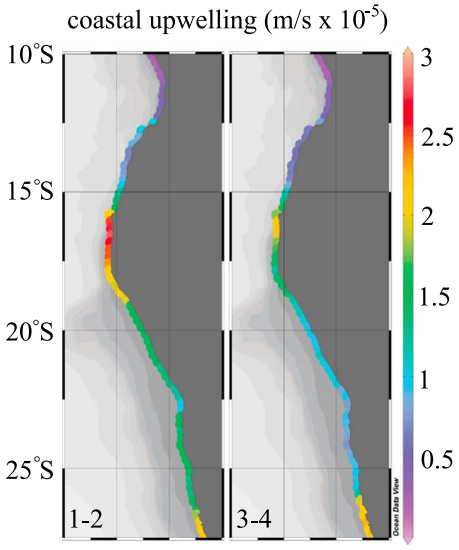

Figure 2. Two week average coastal upwelling rates due to along-shore wind stress. Maps 1–2 and 3–4 coincide with the first and last 2 weeks of the cruise, respectively.

In exemplary chemical profiles from stations 16 and 17, NH_4^+ concentration maxima fell at or just below the MLD and just above the NO_2^- concentration maxima (Figures 5a and 5b). NO_3^- concentrations were lower in the surface water and increased rapidly below the mixed layer (Figure 5c). Transmissometer beam attenuation was generally higher in the surface water and lower below the mixed layer, as expected if particles generated by biological activity in the surface were decaying as they sank out of the mixed layer. However, at station 19 (the station of the northern transect that was closest to the coast), the beam attenuation was also elevated between 200 m and 400 m (Figure 5d), indicating that particles from the sediments may have been resuspended at these depths [*Noble et al.*, 2012; *Lam and Bishop*, 2008]. The depths of particle resuspension at station 19 coincided with the N_2O concentration maximum observed at this and other stations further offshore in the northern transect (Figure 5e), suggesting that some of this N_2O was produced in or near the sediments or in particles resuspended from the sediments along the Angolan continental shelf.

The maximum N_2O concentration was generally observed deeper in the water column (for example, at 299 m depth at station 17, concentration = 49 nM) and had a more enriched isotopic composition ($\delta^{15}N^{bulk} = 5.8 \pm 0.1‰$, $\delta^{18}O = 39.7 \pm 0.1‰$, SP = 9.8 ± 1.0‰) than the N_2O in the isotopic minimum (Figures 5e–5h). At the depth of the N_2O concentration maximum, older water circulating down from the subequatorial Atlantic accumulates nutrients and loses O_2 as it flows along the productive Angolan shelf and then back offshore [*Brea et al.*, 2004]. As a result, N_2O concentrations higher than 40 nM extended off the coast as far as station 11 (Figure 3b).

Below the concentration maximum, the isotopic signatures of N_2O continued to increase as the N_2O concentration decreased. The deepest water sampled (800 m to 1000 m) contained N_2O with some of the highest observed $\delta^{15}N^{bulk}$–N_2O, $\delta^{18}O$–N_2O, and SP values, for example, at 800 m at station 12, $\delta^{15}N^{bulk} - N_2O = 8.7 \pm 0.1‰$, $\delta^{18}O - N_2O = 46.5 \pm 0.2‰$, and SP = 18.7 ± 0.6‰. This water corresponded in salinity, temperature, and silicate concentration [see *Noble et al.*, 2012] to a mixture of South Atlantic Central Water (SACW), Antarctic Intermediate Water (AAIW, depth = 800 m to 1500 m), and Circumpolar Deep Water (CDW, depth = 800 m to 4000 m), which flows northward into the South Atlantic from the Southern Ocean [*Brea et al.*, 2004]. Although this water is oxic, it has undergone significant O_2 consumption since it last fully equilibrated with the atmosphere so that at 800 m at station 12, the observed O_2 concentration was 130 μM while the concentration at atmospheric equilibrium would have been 320 μM. CDW is particularly old and nutrient rich [*Broecker et al.*, 1985; *Poisson and Chen*, 1987] and may have contributed to the O_2 depletion and elevated silicate concentrations that were observed at this depth.

3.2. N_2O Emissions

Atmospheric N_2O fluxes in this region are enhanced by a combination of shallow N_2O production, cyclonic upwelling into the mixed layer, and ventilation of older, mesopelagic water along the coast. N_2O saturation disequilibrium (ΔN_2O) in the mixed layer was highest near the African coast (Figure 4b) with slight undersaturations observed at some of the offshore stations (stations 8, 11, 12, 13, 14, and 16) (Table 1). Average wind speeds were generally higher to the west and north, and gas transfer velocities were correspondingly lower along the southern transect (Figure 4d). The direction of wind stress curl reversed from inducing downwelling (positive wind stress curl) in the western portion of the northern transect to inducing upwelling (negative wind stress curl) at the eastern stations (Figure 4a). Curl-induced upwelling may have been an important mechanism for transferring subsurface N_2O into the mixed layer offshore, while coastal upwelling was the major nearshore mechanism, particularly at the northern coastal stations.

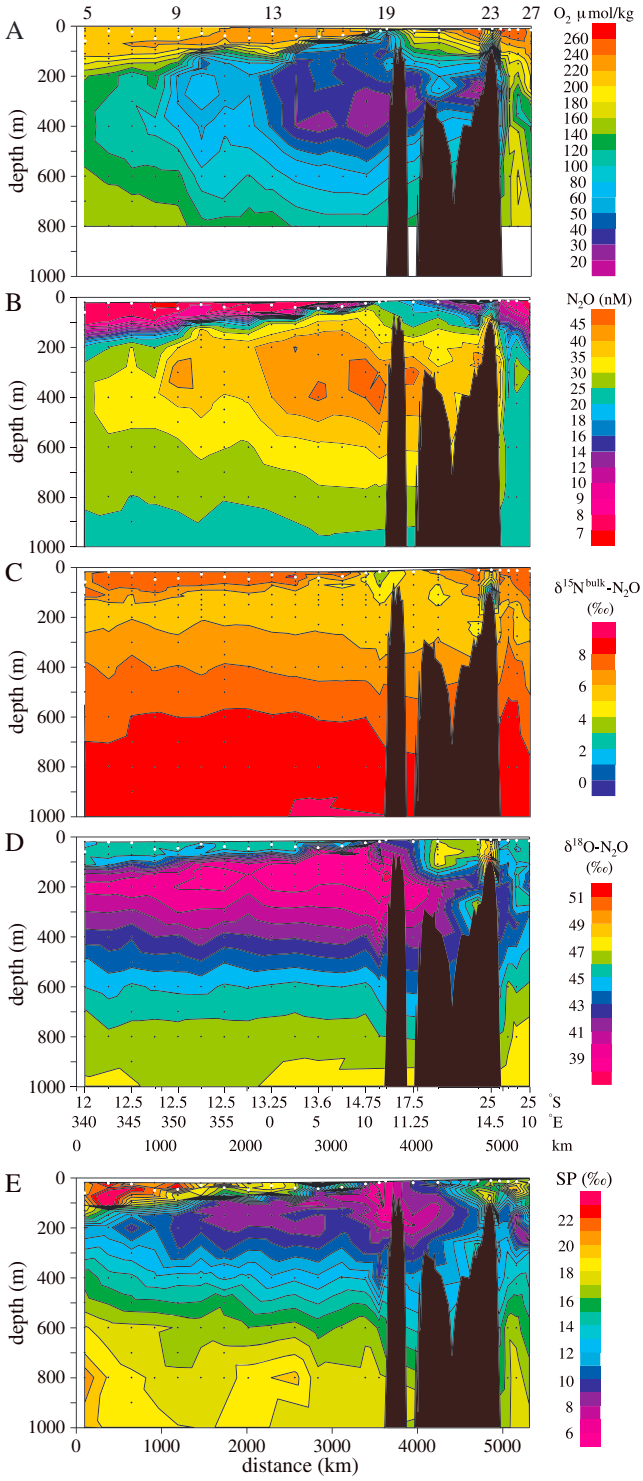

Figure 3. (a) Dissolved O_2, (b) N_2O, (c) $\delta^{15}N^{bulk}$–N_2O, (d) $\delta^{18}O$–N_2O, and (e) SP along each of the three legs of the cruise. White circles indicate the MLD. Black areas represent the sediment depth along the coastal transect.

N_2O fluxes into the atmosphere were highest near the coast, reaching 28 µmol/m^2/d at station 17, 46 µmol/m^2/d at station 18, and 43 µmol/m^2/d at station 20 (Table 1). Fluxes were not calculated at stations 19, 22, and 23 because no measurements were taken above the MLD at these stations, but the oversaturation of N_2O just below the very thin mixed layer at these stations indicates that fluxes were probably also high there. Our flux estimates are similar to the 24 µmol/m^2/d to 36 µmol/m^2/d fluxes reported by *Gutknecht et al.* [2013b] for the region near 23°S between 13.2°E and 14.1°E (closest to stations 22 and 23 in this study) in December 2009. Biogeochemical model simulations of this region produced maximum fluxes as high as 51 µmol/m^2/d near the coast [*Gutknecht et al.*, 2013b], also suggesting that our own calculations are reasonable.

3.3. Shallow N_2O Sources in the Isotopic Minimum

There was a general correspondence between water with high N_2O concentrations and water with high concentrations of NO_3^- relative to PO_4^{3-} (calculated as N* according to *Gruber and Sarmiento* [1997]) (Figure 6), but no strong correlations were observed between the N_2O concentration and N* along the isopycnals that were sampled. Water with high N* values may be a product of local N_2 fixation, as rates of N_2 fixation near the Angolan coast measured during the cruise were comparable to rates measured in the oligotrophic North Atlantic [*Sohm et al.*, 2011]. Stations with relatively high surface N_2 fixation rates (stations 17, 18, 19, and 20) coincided with those that had the most intense shallow N_2O isotopic minima ($\delta^{15}N^{bulk} - N_2O$ = 3.4 ± 0.1‰ − 5.4 ± 0.1‰, $\delta^{18}O - N_2O$ = 37.5 ± 0.2‰ − 39.1 ± 0.2‰, SP = 5.3 ± 0.6‰ − 7.2 ± 0.6‰), suggesting that the release of ^{15}N-depleted organic nitrogen by diazotrophs in this region may have partially contributed to the production of ^{15}N-depleted N_2O.

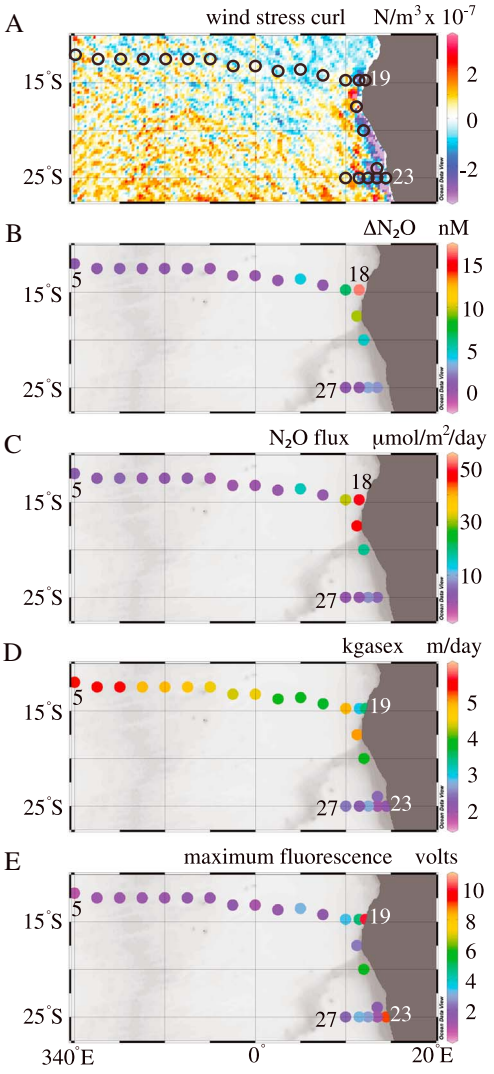

Figure 4. (a) Average wind stress curl for the last 2 weeks of the cruise (negative values favor upwelling), (b) N_2O saturation disequilibria (ΔN_2O) in the mixed layer, (c) N_2O fluxes, (d) 60 day weighted gas transfer velocities (k_{gasex}), and (e) maximum fluorescence.

N_2O produced at the depth of the isotopic minimum is close to the mixed layer and therefore likely to be transferred directly to the atmosphere, making it an important contributor to total marine N_2O emissions to the atmosphere. To estimate the isotopic composition of the shallow biological N_2O source, samples with a salinity ≥35.7 from the northern zonal transect were modeled as a two-component mixture of atmospheric N_2O and N_2O produced by the shallow source. The threshold salinity of 35.7 was chosen to exclude water upwelled along the coast from the deep halocline. The N_2O concentration at the depth of the isotopic minimum ($N_2O_{isotopic\ min}$, units = nM) was modeled as a constant concentration of tropospheric N_2O (N_2O_{trop}) and a variable amount of N_2O produced by a local biological source ($N_2O_{shallow\ source}$):

1. $N_2O_{isotopic\ min} = N_2O_{trop} + N_2O_{shallow\ source}$
2. $\delta^{18}O_{isotopic\ min}\ N_2O_{isotopic\ min} = \delta^{18}O_{trop}\ N_2O_{trop} + \delta^{18}O_{shallow\ source}\ N_2O_{shallow\ source}$
3. $\delta^{15}N^{bulk}_{isotopic\ min}\ N_2O_{isotopic\ min} = \delta^{15}N^{bulk}_{trop}\ N_2O_{trop} + \delta^{15}N^{bulk}_{shallow\ source}\ N_2O_{shallow\ source}$
4. $SP_{isotopic\ min}\ N_2O_{isotopic\ min} = SP_{trop}\ N_2O_{trop} + SP_{shallow\ source}\ N_2O_{shallow\ source}$

The isotopic composition of $N_2O_{shallow\ source}$ was estimated as the *y* intercept of linear regressions of $\delta^{15}N^{bulk}$–N_2O, $\delta^{18}O$–N_2O, and SP versus 1/[N_2O] (Figures S1–S3 in the supporting information).

This approach does not account for N_2O that was horizontally transported or vertically mixed into the surface water. Since wind stress curl varies coherently across the northern section, we grouped the data into three segments based on the average wind stress curl values for the 2 week period prior to each station's sampling date. These values were generally positive (i.e., downwelling) at the western stations (stations 5–8), near zero through the middle stations (stations 9–14), and generally negative at the eastern stations (stations 15–17). We then calculated the isotopic composition of $N_2O_{shallow\ source}$ for each section independently using the two-source model described above. Grouping the stations in this way also split the transect up along the east-west concentration gradient of the deep concentration maximum, thereby creating data subsets that should have relatively large differences in how much upwelling from the concentration maximum influenced the isotopic composition of the N_2O in the isotopic minimum.

The results for each group of stations (Figures S1–S3 in the supporting information) were quite similar for $\delta^{15}N^{bulk}$–N_2O and $\delta^{18}O$–N_2O, with the $\delta^{15}N^{bulk}$–N_2O ranging from 4.2 ± 0.3‰ at stations 5–8, 3.9 ± 0.2‰ at stations 9–14, and 3.9 ± 0.1‰ at stations 15–17 and the $\delta^{18}O$–N_2O ranging from 36.2 ± 0.5‰ at stations 5–8, 36.7 ± 0.4‰ at stations 9–14, and 36.7 ± 0.5‰ at stations 15–17. The SP signatures decreased slightly heading into the upwelling zone, with values of 6.0 ± 2.0‰ at stations 5–8, 5.2 ± 1.8‰ at stations 9–14, and 4.3 ± 1.3‰ at stations 15–17. Values are given with the 95% confidence intervals of the fit coefficients from the linear regressions. Among the three data subsets, there is not a systematic variation in the calculated isotopic composition of $N_2O_{shallow\ source}$ that we can attribute to changes in the contribution of N_2O from the concentration maximum to the N_2O in the isotopic minimum. That is, despite increased upwelling and a

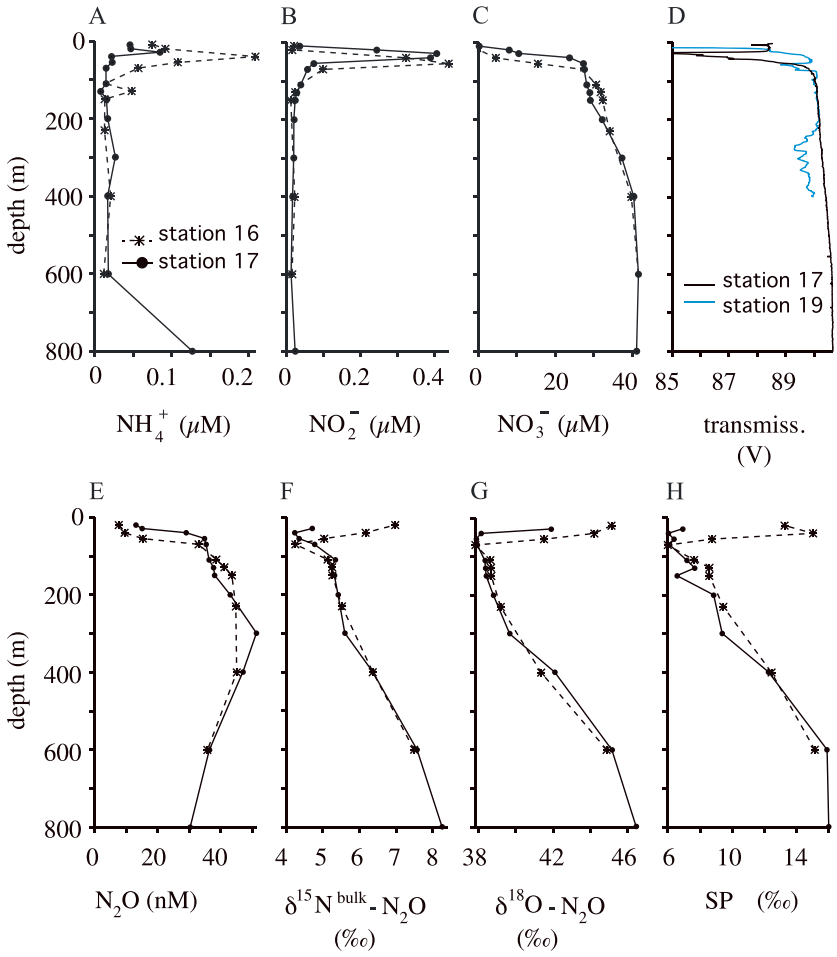

Figure 5. (a) NH_4^+, (b) NO_2^-, (c) NO_3^-, (d) transmissometer beam attenuation, (e) N_2O, (f) $\delta^{15}N^{bulk}$–N_2O, (g) $\delta^{18}O$–N_2O, and (h) SP. All profiles are from stations 16 and 17 except in Figure 5d.

more intense N_2O concentration maximum to the east, the $\delta^{15}N^{bulk}$–N_2O, $\delta^{18}O$–N_2O, and SP estimated for the shallow source do not increase from west to east, as we would expect them to if N_2O from the concentration maximum influenced the isotopic signatures of the N_2O in the isotopic minimum. Furthermore, the shallow source signatures calculated here are similar to those calculated by *Popp et al.* [2002] for the N_2O isotopic minimum observed at 200 m to 300 m at station ALOHA in the north Pacific Gyre, where $\delta^{15}N^{bulk} - N_2O = 3.7 \pm 0.9$‰, $\delta^{18}O - N_2O = 37.2 \pm 1.9$‰, and SP = 1.1‰ to 2.7‰. Nevertheless, if upwelling of N_2O from the concentration maximum (for example, 299 m at station 17) had contributed 5% of the N_2O that we are attributing to the shallow source at stations 15–17, then the actual isotopic composition of $N_2O_{shallow\ source}$ should be revised down to $\delta^{15}N^{bulk} - N_2O = 3.6 \pm 0.1$‰, $\delta^{18}O - N_2O = 34.6 \pm 0.6$‰, and SP = 3.8 ± 1.5‰. If the concentration maximum had contributed 10% of the N_2O, then the $N_2O_{shallow\ source}$ signatures would be lowered further to $\delta^{15}N^{bulk} - N_2O = 3.3 \pm 0.1$‰, $\delta^{18}O - N_2O = 32.3 \pm 0.6$‰, and SP = 3.2 ± 1.5‰.

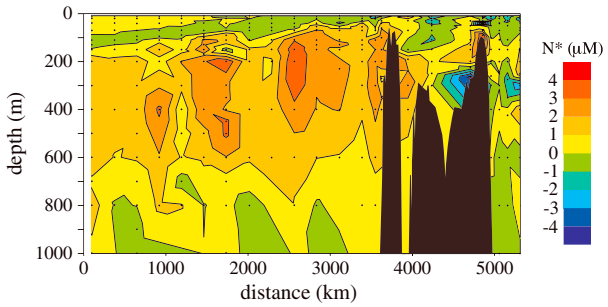

Figure 6. N* values along each of the three legs of the cruise.

Ammonia-oxidizing microorganisms are the likely source of the isotopically depleted N_2O produced in the shallow

isotopic minimum. This N_2O was found in oxygenated water at the base of the mixed layer and generally coincided with the top of the nutricline, a depth at which previous studies have noted maxima in the rates of NH_3 oxidation and the abundance of ammonia oxidizers [*Ward et al*., 1982; *Beman et al*., 2008; *Santoro et al*., 2010] and at which we observed small NH_4^+ and NO_2^- concentration maxima at a number of cruise stations (Figures 5a and 5b). Both bacterial and archaeal ammonia oxidizers produce N_2O [*Ritchie and Nicholas*, 1972; *Santoro et al*., 2011; *Löscher et al*., 2012]. Ammonia-oxidizing bacteria produce N_2O through the decomposition of hydroxylamine (NH_2OH), an intermediate during NH_3 oxidation to NO_2^-, and also through an enzyme-mediated process known as nitrifier denitrification, which reduces NO_2^- to N_2O [*Hooper and Terry*, 1979; *Poth and Focht*, 1985]. In order to distinguish and quantify the contributions of these two pathways to the shallow N_2O source, we have focused our analysis on its SP signature since this is distinct for N_2O produced by either pathway and in either case is believed to be independent of the substrates' isotopic composition [*Toyoda et al*., 2002; *Schmidt et al*., 2004]. The SP of N_2O produced by NH_2OH decomposition can be as high as 36‰, while nitrifier denitrification produces N_2O with a much lower SP, possibly as low as −10.7‰ [*Sutka et al*., 2006; *Frame and Casciotti*, 2010]. N_2O produced by archaeal ammonia oxidizers living in aerobic conditions appears to derive from the NH_2OH pathway and has a SP (30.3‰) that is close to that of NH_2OH decomposition by bacterial ammonia oxidizers [*Santoro et al*., 2011]. It is possible but not yet proven that archaeal ammonia oxidizers also produce low-SP N_2O. If the SP of the N_2O produced in the isotopic minimum of the South Atlantic is a two-component mixture of N_2O produced by nitrifier denitrification and NH_2OH decomposition, and we use the end-member SP values estimated by *Frame and Casciotti* [2010] for a bacterial ammonia oxidizer ($SP_{\text{nitrifier denitrification}} = -10.7‰$ and $SP_{\text{NH2OH decomposition}} = 36.3‰$), then NH_2OH decomposition is estimated to have contributed between 36% (0.29 = (−10.7‰ − 6.0‰)/(−10.7‰ − 36.3‰)) and 32% (0.32 = (−10.7‰ − 4.3‰)/(−10.7‰ − 36.3‰)) of the N_2O source in the shallow isotopic minimum, while nitrifier denitrification contributed the remaining 64% to 68%.

3.4. Sources of the N_2O Concentration Maximum

N_2O concentrations were highest between 200 m and 400 m at the coastal stations of the northern transect. The subequatorial branch of SACW is ventilated more slowly and has higher rates of organic matter remineralization than the subtropical branch of SACW [*Brea et al*., 2004] so that the water of the northern transect probably had a larger inventory of remineralized NO_3^- and N_2O, as well as a depleted O_2 inventory, by the time it entered the coastal upwelling region where we observed it. Production of this "extracoastal" N_2O was most likely a by-product of NH_3 oxidation and nitrifier denitrification fueled by the rain of organic nitrogen out of the mixed layer, in a manner consistent with the classical view of N_2O production in oxygenated water [*Yoshinari*, 1976; *Cohen and Gordon*, 1979; *Nevison et al*., 2003].

The shallow continental shelf in this region, which supports denitrification and anammox as well as NH_3 oxidation and NO_2^- oxidation [*Füssel et al*., 2012], is probably also a zone of accelerated N_2O production. The isotopic composition of the N_2O in the concentration maximum near the coast is consistent with production by diffusion-limited denitrification and/or nitrifier denitrification of NO_2^-, which we might expect to find associated with the coastal sediments, the benthic boundary layer above the sediments, or particles resuspended from the sediments. Specifically, the $\delta^{15}N^{bulk}$–N_2O (5.7‰ to 6.6‰) was similar to that of NO_3^- ($\delta^{15}N - NO_3^-$ = 5‰ to 6‰ (Casciotti et al., in preparation, 2014)), while the $\delta^{18}O$–N_2O (40‰ to 42‰) was significantly higher than the $\delta^{18}O$–NO_3^- (2‰ to 3‰ (Casciotti et al., in preparation, 2014)) and also higher than the $\delta^{18}O$–N_2O of the shallow N_2O source (36.2‰ to 36.7‰). This pattern of low $\delta^{15}N^{bulk}$–N_2O and high $\delta^{18}O$–N_2O relative to $\delta^{15}N$–NO_3^- and $\delta^{18}O$–NO_3^-, respectively, suggests that the N_2O was produced in a system where the rates of the enzymatic reduction reactions carried out by denitrifiers (NO_3^- ➔ NO_2^- ➔ nitric oxide (NO) ➔ N_2O exceed that of substrate supply. Since diffusion typically has a very small isotope effect, diffusion limitation can eliminate expression of the enzymes' typically much larger kinetic isotope effects so that the net isotope effect is close to 0‰ [see *Farquhar et al*., 1982; *Jinuntuya-Nortman et al*., 2008]. When the rates of these reduction reactions are not limited by diffusion, full expression of the kinetic isotope effects of NO_3^- reduction produces NO_2^- that is depleted in ^{15}N relative to the substrate NO_3^- [*Barford et al*., 1999; *Granger et al*., 2006, 2008; *Kritee et al*., 2012] and subsequent reduction of this NO_2^- produces N_2O that is also depleted in ^{15}N relative to the NO_2^- and NO_3^- [*Bryan et al*., 1983]. However, this does not bear out at the depths of the N_2O concentration maximum, where $\delta^{15}N^{bulk}$–N_2O and $\delta^{15}N$–NO_3^- were actually quite similar, as mentioned above.

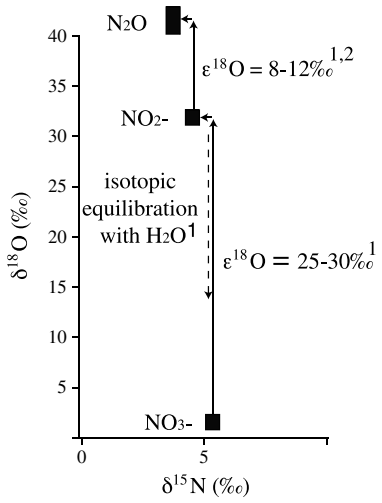

Figure 7. N_2O production in a system where NO_3^- reduction is diffusion limited. Branching isotope effects ($\varepsilon^{18}O$) are expressed even though kinetic isotope effects are not expressed. The N_2O that results from NO_3^- reduction is more enriched in ^{18}O and has similar $\delta^{15}N$ values compared to the substrate NO_3^-. [1]*Casciotti et al.* [2007], [2]*Frame and Casciotti* [2010].

The $\delta^{18}O$–N_2O (40‰ to 42‰), however, is significantly *higher* than the $\delta^{18}O$–NO_3^- (2‰ to 3‰), even though the large kinetic isotope effects that favor reduction of ^{16}O–NO_3^- over ^{18}O–NO_3^- [*Granger et al.*, 2006] must be similarly suppressed when denitrification is diffusion limited. The discrepancy is explained by the fact that a branching isotope effect, which favors the removal of ^{16}O relative to ^{18}O as NO_3^- is reduced to NO_2^-, is expressed even when diffusion limits NO_3^- reduction rates and thus expression of the O kinetic isotope effects. The branching isotope effect for NO_3^- reduction to NO_2^- is as high as 25–30‰ [*Casciotti et al.*, 2007] (Figure 7). The remaining gap between $\delta^{18}O$–NO_3^- and $\delta^{18}O$–N_2O can be explained by another branching isotope effect of 10–12‰ associated with NO_2^- reduction to N_2O by denitrification [*Casciotti et al.*, 2007] or possibly the 8.4‰ effective isotope effect reported for NO_2^- reduction to N_2O during nitrifier denitrification [*Frame and Casciotti*, 2010]. Sediments are known to provide an environment that suppresses expression of the large enzymatic kinetic isotope effects associated with NO_3^- and O_2 consumption [*Brandes and Devol*, 1997]. In the water column, large particles have similarly been proposed as an environment that supports rapid O_2 consumption without accompanying isotopic enrichment of the remaining O_2 [*Ostrom et al.*, 2014].

There are other potential influences on the isotopic composition of N_2O produced by NO_3^- reduction, including the O isotopic equilibration of NO_2^- with water, which is dependent on ambient temperature and pH [*Buchwald and Casciotti*, 2013]. Biological NO_2^- fluxes measured by *Füssel et al.* [2012] in the benthic boundary layer of this region suggest that the residence time of NO_2^- in this zone may be on the order of 5–10 days and is probably faster if physical fluxes are taken into account. Since abiotic O isotopic equilibration is relatively slow at seawater pH [*Buchwald and Casciotti*, 2013], we expect this effect to be relatively minor, although we cannot rule out the possibility of faster enzymatically catalyzed exchange. Another consideration is that once NO_2^- is produced, it may also be oxidized to NO_3^- by nitrite oxidizers or reduced to N_2 by anammox [*Füssel et al.*, 2012]. While we cannot constrain how these processes affect the isotopic composition of NO_2^- (and therefore N_2O) without additional information about their rates, spatial distributions, and isotope effects, the fact remains that we can close the isotope gap between NO_3^- and N_2O by invoking only denitrification and possibly also nitrifier denitrification of NO_2^-.

The SP of the N_2O in the concentration maximum (SP = 9.8% at 299 m at station 17; see Figure 8a) was somewhat higher than what has been reported for N_2O that is produced by denitrification or nitrifier denitrification (−0.5 to −5‰ [*Toyoda et al.*, 2005; *Sutka et al.*, 2006] and −10.7‰ [*Frame and Casciotti*, 2010], respectively). A background atmospheric N_2O equilibrium concentration of 8.5 nM to 11 nM with a SP of 18.7 ± 2.2‰ [*Yoshida and Toyoda*, 2000] could contribute to, but does not fully explain, the higher SP values of the N_2O in this water. Therefore, the higher SP signature must also reflect N_2O production by NH_2OH decomposition during NH_3 oxidation or partial N_2O consumption by denitrification in the water column. We favor the first explanation, one of NH_2OH decomposition, which could have occurred locally or in the water mass before it entered our study region. It seems likely that oxidation of NH_3 diffusing out of the sediments of the continental shelf would be significant, and rather unlikely that dissolved O_2 concentrations dropped low enough, for long enough, over a large enough portion of the water column to support N_2O consumption by denitrification in the bulk phase. The threshold O_2 concentrations at which denitrifiers begin to first produce and then consume N_2O are low but still relatively uncertain. In a model of the Benguela region, *Gutknecht et al.* [2013a] assumed that NO_3^- reduction does not proceed when O_2 is above 25 μM, while the transition from N_2O production to N_2O consumption by denitrification appears to occur as O_2 drops below 10 μM in the Pacific

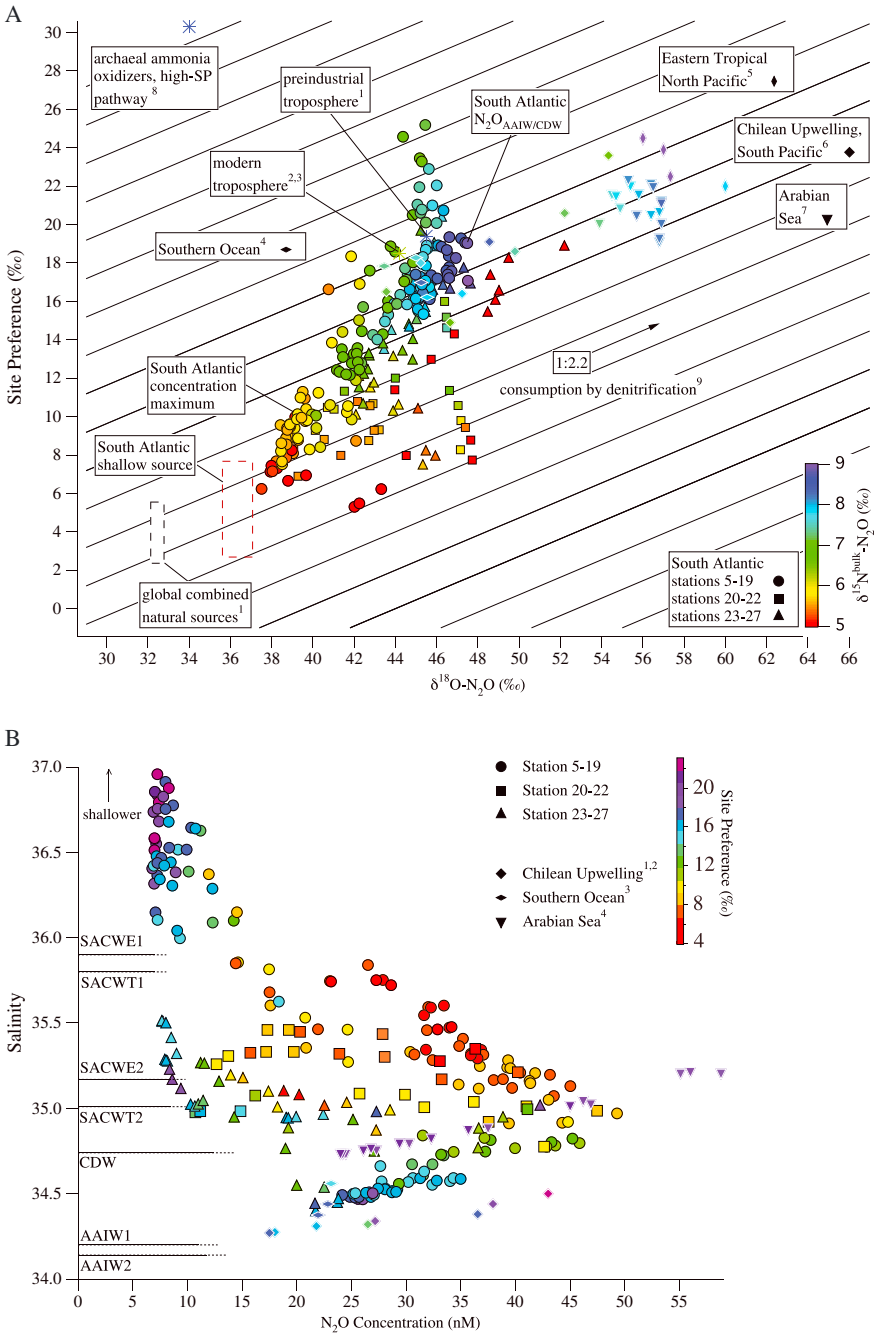

Figure 8. (a) SP versus $\delta^{18}O$–N_2O measurements of South Atlantic N_2O are represented as circles for the northern leg, squares for the coastal leg, and triangles for the southern leg. Isolines have a 1:2.2 slope that reflects the ratios of the isotope effects that govern SP and $\delta^{18}O$–N_2O during N_2O consumption by denitrifier cultures, as measured by *Ostrom et al.* [2007]. Data from previous studies are from [1]*Park et al.* [2012], [2]*Yoshida and Toyoda* [2000], [3]*Kim and Craig* [1990], [4]*Boontanon et al.* [2010], [5]*Yamagishi et al.* [2007], [6]*Charpentier et al.* [2007], [7]*McIlvin and Casciotti* [2010], [8]*Santoro et al.* [2011], and [9]*Ostrom et al.* [2007]. Although we have included high-SP N_2O from archaeal ammonia oxidizers, it is possible but not known whether they also produce N_2O with a low SP value. The $\delta^{15}N^{bulk}$–N_2O estimated for the global combined natural sources by *Park et al.* [2012] was -5.3 ± 0.2‰ and is off the color scale used here. (b) Salinity versus N_2O concentration for all stations. The preindustrial (275 ppb) and modern (319 ppb) atmospheric equilibrium concentrations are given by the lengths of the solid and dashed lines, respectively, for the major branches of South Atlantic Central Water (SACWE1, SACWE2, SACWT1, and SACWT2), Circumpolar Deep Water (CDW), and Antarctic Intermediate Water (AAIW1 and AAIW2) as defined by *Brea et al.* [2004]. Data not measured during this study include [1]*Charpentier et al.* [2007], [2]*Charpentier et al.* [2010], [3]*Boontanon et al.* [2010], and [4]*McIlvin and Casciotti* [2010] (with unpublished salinity data). Salinity decreases with increasing depth for all locations except the Southern Ocean.

[*Zamora et al.*, 2012]. Measured O_2 concentrations in the water column during this study were generally above both these values but did drop as low as 19 μM at 300 m at station 17 and 11 μM at 110 m at station 23.

Although we argue against N_2O consumption in the water column, our observations do not rule out N_2O reduction in the sediments. N_2O consumption within the sediments is likely to be diffusion limited and/or involve complete consumption of any N_2O made in the sediments or diffusing into the sediments from the overlying water. This is analogous to the underexpression of kinetic isotope effects during NO_3^- reduction in high reactivity sediments, where rapid denitrification rates nearly completely consume NO_3^- within the sediments and therefore do not contribute to isotopic enrichment of NO_3^- in the overlying water [*Brandes and Devol*, 1997; *Lehmann et al.*, 2004, 2007]. If sedimentary N_2O consumption behaves similarly to NO_3^- consumption, then it would not produce strong isotopic enrichment of N_2O dissolved in the water column, even if rapid sedimentary N_2O reduction is occurring.

There is no obvious NO_3^- deficit in the water that contains the N_2O concentration maximum. If sedimentary or water column denitrification was an important removal mechanism for fixed nitrogen at these depths, one might expect N* values to be low [*Gruber and Sarmiento*, 1997] (see Figure 6). However, our proposed mechanism of benthic-/sediment-associated N_2O production is decoupled from the effects of denitrification on N* by the fact that NO_3^- reduction by denitrifiers does not necessarily always proceed to completion (i.e., to N_2). Reduction of NO_3^- to NO_2^- followed by reduction of a fraction of this NO_2^- to N_2O by denitrification and/or nitrifier denitrification could proceed without changing N* very much if the remaining NO_2^- is then reoxidized to NO_3^- by nitrite-oxidizing nitrifiers. Furthermore, N* is calculated on a micromolar scale that is probably not precise enough to capture the nanomolar decrease in NO_3^- concentration that would be needed to produce the N_2O in the concentration maximum. In other words, N_2O concentrations need not bear any obvious relationship to N*. In the benthic boundary layer, spatial coupling of NO_3^- reduction to NO_2^- by denitrifiers to rapid NH_3 and NO_2^- oxidation by nitrifiers could explain how water carrying high N_2O concentrations can be advected off the continental shelf without also carrying high concentrations of NH_4^+ and NO_2^- or major N* depletions. In fact, some of the highest observed N* values coincide with the N_2O concentration maximum (Figure 6), suggesting that remineralization of N-rich organic matter may outweigh any fixed-N loss through denitrification or anammox. Finally, microbial formation of apatite is an important sedimentary sink for PO_4^{3-} in this region [*Goldhammer et al.*, 2010] and may also push N* values higher along the continental shelf.

3.5. Deep N_2O Sources and Transport

Moving deeper through the water column, from the concentration maximum down to the deepest depths analyzed here (800 m to 1000 m), the $\delta^{15}N^{bulk}$–N_2O, $\delta^{18}O$–N_2O, and SP signatures continued to increase. The deepest samples derived from AAIW and CDW and contained N_2O with an isotopic composition that was similar to preindustrial tropospheric N_2O [*Park et al.*, 2012], but concentrations that were substantially higher than either the modern or preindustrial equilibrium N_2O concentrations. For example, the isotopic composition of preindustrial tropospheric N_2O is estimated to have been $\delta^{15}N^{bulk} - N_2O = 9.3 \pm 0.2$‰, $\delta^{18}O - N_2O = 45.5 \pm 0.2$‰, and SP = 19.4 ± 1.5‰ [*Park et al.*, 2012] and at 800 m at station 12, $\delta^{15}N^{bulk} - N_2O = 8.7 \pm 0.1$‰, $\delta^{18}O - N_2O = 46.5 \pm 0.2$‰, and SP = 18.7 ± 0.6‰ ($N_2O_{AAIW/CDW}$ in Figure 8a), yet the N_2O concentration at this depth was 25.4 nM, about twice as high as either the modern or preindustrial equilibrium N_2O concentrations (12.8 nM and 11.0 nM, respectively; see Figure 8b). Therefore, at these depths there must have been another source of N_2O in addition to the atmosphere.

$N_2O_{AAIW/CDW}$ has higher $\delta^{15}N^{bulk}$–N_2O, $\delta^{18}O$–N_2O, and SP values than the shallow N_2O source(s) that were observed above it (Figure 8a). $N_2O_{AAIW/CDW}$ is also more isotopically enriched than expected for the N_2O produced by NH_2OH decomposition, nitrifier denitrification, and denitrification [*Barford et al.*, 1999; *Sutka et al.*, 2006; *Toyoda et al.*, 2005; *Frame and Casciotti*, 2010]. N_2O consumption by denitrifying bacteria involves large kinetic isotope effects and is the only known biological process that simultaneously enriches N_2O in ^{15}N, ^{18}O, and SP [*Barford et al.*, 1999; *Menyailo and Hungate*, 2006; *Ostrom et al.*, 2007]. Wherever this process plays a role in the N_2O cycle and is not limited by diffusion [*Jinuntuya-Nortman et al.*, 2008], it increases the $\delta^{15}N^{bulk}$–N_2O, $\delta^{18}O$–N_2O, and SP signatures of the remaining N_2O by favoring the reduction of $^{14}N_2O$ over $^{15}N_2O$, $N_2{}^{16}O$ over $N_2{}^{18}O$, and $^{15}N^{14}NO$ over $^{14}N^{15}NO$ [e.g., *Westley et al.*, 2006; *Yamagishi et al.*, 2007; *Sasaki*

et al., 2011]. These increases in isotopic signatures occur in constant proportions to one another, with $\delta^{18}O$–N_2O increasing by 2.2‰ with every 1‰ increase in SP, and by 2.5–2.6‰ with every 1‰ increase in $\delta^{15}N^{bulk}$–N_2O [*Menyailo and Hungate*, 2006; *Ostrom et al*., 2007; *Jinuntuya-Nortman et al*., 2008]. On an isotope-isotope plot, the data reported here tend to lie away from these constant proportions, with $\delta^{18}O$–N_2O increasing by a smaller amount relative to SP and $\delta^{15}N^{bulk}$–N_2O (Figure 8a). As discussed below, this fact is likely tied to this water's history of mixing and long-range horizontal transport.

N_2O consumption by local water column denitrification in the South Atlantic is not a likely explanation for the observed isotopic enrichment of this N_2O because ambient O_2 concentrations at these depths (120–150 μM) were too high to support denitrification. However, the mesopelagic South Atlantic may receive water from remote zones of water column denitrification, including the Indian Ocean via eddies derived from the Agulhas Current [*Hutchings et al*., 2009], and from the eastern South Pacific via the Peru-Chile Undercurrent and the Drake Passage [*Tsuchiya et al*., 1994]. The Southern Ocean recirculates water and nutrients from the thermocline waters of all the southern ocean basins [*Sarmiento et al*., 2004], partially balancing Atlantic meridional overturning circulation by exporting AAIW and CDW back into the South Atlantic [*Broecker et al*., 1998; *Marshall and Speer*, 2012]. This flow of water likely contributes to the relatively high N_2O concentrations and $\delta^{15}N^{bulk}$–N_2O, $\delta^{18}O$–N_2O, and SP values observed at 800 m to 1000 m in the South Atlantic. Indeed, the shallow Southern Ocean (150 m to 300 m, 140°E, 61°S) has a similar N_2O concentration and isotopic composition (concentration = ~23 nM, $\delta^{15}N^{bulk} - N_2O = 7.6 \pm 0.3$‰, $\delta^{18}O - N_2O = 44.7 \pm 1.1$‰, and SP =$17.4 \pm 1.1$‰) [*Boontanon et al*., 2010] to that of $N_2O_{AAIW/CDW}$ (Figure 8a).

The salinity range of the water carrying $N_2O_{AAIW/CDW}$ and the N_2O concentration maximum in the South Atlantic is similar to that of subsurface water in the Chilean Upwelling Zone (400 m to 800 m) [*Charpentier et al*., 2007], deeper water in the Arabian Sea (1200 m to 3000 m) (*McIlvin and Casciotti* [2010] with unpublished salinity data), and the shallow Southern Ocean (150 m to 300 m) [*Boontanon et al*., 2010] (Figure 8b). Some of the deeper N_2O in the South Atlantic may therefore be exported from a major water column denitrification zone in one of the other ocean basins via the Southern Ocean. This would be consistent with findings that N_2O produced deeper in the water column may be transported thousands of kilometers from its point of formation [*Nevison et al*., 2003]. Long-range N_2O transport, particularly through the Southern Ocean, would also give this ODZ water an opportunity to mix with higher-O_2 water, thus explaining our observation that at 800 m to 1000 m, the water in the South Atlantic has a relatively high O_2 concentration but also contains N_2O with the isotopic imprint of N_2O consumption by water column denitrification.

The isotopic composition of $N_2O_{AAIW/CDW}$ lies near a mixing line between the N_2O in the concentration maximum of the South Atlantic and the N_2O observed in the Chilean Upwelling Zone (400 m to 800 m) [*Charpentier et al*., 2007], the Arabian Sea (1200 m to 3000 m) [*McIlvin and Casciotti*, 2010], and the Eastern Tropical North Pacific (800 m to 1200 m) [*Yamagishi et al*., 2007] (Figure 8a). The departure of $N_2O_{AAIW/CDW}$ from this mixing line might be explained in part by an additional contribution of N_2O from tropospheric N_2O. However, production of high-SP N_2O by ammonia oxidizers may have also driven the observations away from a perfectly straight mixing line.

4. Conclusions

The coastal upwelling region along southwestern Africa is an important hotspot of marine N_2O release in the South Atlantic. Atmospheric N_2O fluxes of up to 46 μmol/m^2/d were estimated at stations along the coast of Angola and Namibia. In the top 1000 m of the water column, shallower N_2O was more depleted in ^{15}N and ^{18}O and had a lower SP than the deeper N_2O. The N_2O concentration maximum was between 200 m and 400 m and fell below the isotopic minimum, which was located in the top 200 m of the water column at all stations. The relatively low SP of the N_2O in the isotopic minimum suggests that this N_2O was produced mainly by nitrifier denitrification, carried out by ammonia oxidizers just below the mixed layer. The observed N_2O concentration maximum was highest in the northern transect (14.75°S), near the Angolan coast, where a combination of aged subequatorial SACW, a highly productive upwelling zone, and sediment-associated denitrification and nitrifier denitrification are all likely to have contributed to the high N_2O concentrations that were observed. We attribute the relatively enriched isotopic composition of the N_2O between 800 m and 1000 m to N_2O exported out of an ODZ in another ocean basin, such as the South Pacific or the Indian Ocean.

The isotopic differences among the shallow N_2O source, the concentration maximum, and the deeper N_2O may be useful in investigating how the balance of deep N_2O ventilation and shallow N_2O production influences seasonal cycles and longer-term trends in the isotopic composition of N_2O released to the atmosphere by the ocean.

Acknowledgments
The data for this paper are available under the CoFeMUG program at http://www.bco-dmo.org. We thank the captain and crew of the R/V *Knorr* and chief scientist Mak Saito as well as Abigail Noble, Alysia Cox, Tyler Goepfert, and Chad Hammerschmidt for assistance during the cruise. We also thank Matt McIlvin for expert assistance analyzing samples and Rachel Stanley for generously providing the MATLAB code for calculating gas transfer velocities from QuikSCAT wind data. Reviews from Marian Westley and Nathaniel Ostrom greatly improved the quality of the manuscript. Support for this work came from NSF/OCE grant 05-26277 to K.L.C. and a grant from the MIT EAPS Houghton Fund to C.H.F.

References

Barford, C. C., J. Montoya, M. A. Altabet, and R. Mitchell (1999), Steady-state nitrogen isotope effects of N_2 and N_2O production in *Paracoccus denitrificans*, *Appl. Environ. Microbiol.*, *65*(3), 989–994.

Battle, M., et al. (1996), Atmospheric gas concentrations over the past century measured in air from firn at the South Pole, *Nature*, *383*, 231–235.

Beman, M. J., B. N. Popp, and C. A. Francis (2008), Molecular and biogeochemical evidence for ammonia oxidation by marine Crenarchaeota in the Gulf of California, *ISME J.*, *2*, 429–441.

Boontanon, N., S. Watanabe, T. Odate, and N. Yoshida (2010), Production and consumption mechanisms of N_2O in the Southern Ocean revealed from its isotopomer ratios, *Biogeosci. Discuss.*, *7*, 7821–7848.

Bourassa, M. A., D. M. Legler, J. J. O'Brien, and S. R. Smith (2003), SeaWinds validation with research vessels, *J. Geophys. Res.*, *108*(C2), 3019, doi:10.1029/2001JC001028.

Brandes, J. A., and A. H. Devol (1997), Isotopic fractionation of oxygen and nitrogen in coastal marine sediments, *Geochim. Cosmochim. Acta*, *61*(9), 1793–1801.

Brea, S., X. A. Alvarez-Salgado, M. Alvarez, F. F. Perez, L. Memery, H. Mercier, and M. J. Messias (2004), Nutrient mineralization rates and ratios in the eastern South Atlantic, *J. Geophys. Res.*, *109*, C05030, doi:10.1029/2003JC002051.

Broecker, S. W., T. Takahashi, and T. Takahashi (1985), Sources and flow patterns of deep-ocean waters as deduced from potential temperature, salinity, and initial phosphate concentration, *J. Geophys. Res.*, *90*(C4), 6925–6939, doi:10.1029/JC090iC04p06925.

Broecker, W. S., et al. (1998), How much deep water is formed in the Southern Ocean?, *J. Geophys. Res.*, *103*(C8), 15,833–15,843, doi:10.1029/98JC00248.

Bryan, B. A., G. Shearer, J. L. Skeeters, and D. H. Kohl (1983), Expression of the nitrogen isotope effect associated with denitrification of nitrite, *J. Biol. Chem.*, *258*(14), 8613–8617.

Buchwald, C., and K. L. Casciotti (2013), Isotopic ratios of nitrite as tracers of the sources and age of oceanic nitrite, *Nat. Geosci.*, *6*(4), 308–313, doi:10.1038/NGEO1745.

Casciotti, K. L., J. K. Bohlke, M. McIlvin, S. J. Mroczkowski, and J. E. Hannon (2007), Oxygen isotopes in nitrite: Analysis, calibration, and equilibration, *Anal. Chem.*, *79*, 2427–2436.

Chapman, P., and L. V. Shannon (1987), Seasonality in the oxygen minimum layers at the extremities of the Benguela system, *South Afr. J. Mar. Sci.*, *5*, 85–94.

Charpentier, J., L. Farias, N. Yoshida, N. Boontanon, and P. Raimbault (2007), Nitrous oxide distribution and its origin in the central and eastern South Pacific Subtropical Gyre, *Biogeosciences*, *4*, 729–741.

Charpentier, J., L. Farias, and O. Pizarro (2010), Nitrous oxide fluxes in the central and eastern South Pacific, *Global Biogeochem. Cycles*, *24*, GB3011, doi:10.1029/2008GB003388.

Codispoti, L. A., and J. P. Christensen (1985), Nitrification, denitrification and nitrous oxide cycling in the eastern tropical South Pacific Ocean, *Mar. Chem.*, *16*, 277–300.

Cohen, Y., and L. I. Gordon (1978), Nitrous oxide in the oxygen minimum of the eastern tropical North Pacific: Evidence for its consumption during denitrification and possible mechanisms for its production, *Deep Sea Res.*, *25*, 509–524.

Cohen, Y., and L. I. Gordon (1979), Nitrous oxide production in the ocean, *J. Geophys. Res.*, *84*(C1), 347–353, doi:10.1029/JC084iC01p00347.

Davidson, E. A. (2009), The contribution of manure and fertilizer nitrogen to atmospheric nitrous oxide since 1860, *Nat. Geosci.*, *2*(9), 659–662, doi:10.1038/ngeo608.

Davidson, E. A., F. Y. Ishida, and D. C. Nepstad (2004), Effects of an experimental drought on soil emissions of carbon dioxide, methane, nitrous oxide, and nitric oxide in a moist tropical forest, *Global Change Biol.*, *10*, 718–730, doi:10.1111/j.1529-8817.2003.00762.x.

Davidson, E. A., D. C. Nepstad, F. Y. Ishida, and P. M. Brando (2008), Effects of an experimental drought and recovery on soil emissions of carbon dioxide, methane, nitrous oxide, and nitric oxide in a moist tropical forest, *Global Change Biol.*, *14*, 2582–2590, doi:10.1111/j.1365-2486.2008.01694.x.

De Boyer Montégut, C., G. Madec, A. S. Fischer, A. Lazar, and D. Iudicone (2004), Mixed layer depth over the global ocean: An examination of profile data and a profile-based climatology, *J. Geophys. Res.*, *109*, C12003, doi:10.1029/2004JC002378.

Denman, K. L., et al. (2007), in *Climate Change 2007: The Physical Science Basis*, edited by S. Solomon et al., Cambridge Univ. Press, New York.

Deutsch, C., H. Brix, T. Ito, H. Frenzel, and L. Thompson (2011), Climate-forced variability of ocean hypoxia, *Science*, *333*(6040), 336–9, doi:10.1126/science.1202422.

Elkins, J. W., S. Wofsy, M. B. McElroy, C. E. Kolb, and W. A. Kaplan (1978), Aquatic sources and sinks for nitrous oxide, *Nature*, *275*, 602–606.

Farquhar, G. D., M. H. O'Leary, and J. A. Berry (1982), On the relationship between carbon isotope discrimination and the intercellular carbon dioxide concentration in leaves, *Aust. J. Plant Physiol.*, *9*, 121–137.

Firestone, M. K., R. B. Firestone, and J. M. Tiedje (1980), Nitrous oxide from soil denitrification: Factors controlling its biological production, *Science*, *208*(4445), 749–751.

Fluckiger, J., A. Dallenbach, T. Blunier, B. Stauffer, T. F. Stocker, D. Raynaud, and J.-M. Barnola (1999), Variations in atmospheric N_2O concentration during abrupt climatic changes, *Science*, *285*, 227–230.

Fluckiger, J., et al. (2002), High-resolution Holocene N_2O ice core record and its relationship, *Global Biogeochem. Cycles*, *16*(1), 1010, doi:10.29/2001GB001417.

Fluckiger, J., T. Blunier, B. Stauffer, J. Chappellaz, R. Spahni, K. Kawamura, J. Schwander, T. F. Stocker, and D. Dahl-Jensen (2004), N_2O and CH_4 variations during the last glacial epoch: Insight into global processes, *Global Biogeochem. Cycles*, *18*, GB1020, doi:10.1029/2003GB002122.

Frame, C. H., and K. L. Casciotti (2010), Biogeochemical controls and isotopic signatures of nitrous oxide production by a marine ammonia-oxidizing bacterium, *Biogeosciences*, *7*, 2695–2709.

Fujii, A., S. Toyoda, O. Yoshida, S. Watanabe, K. Sasaki, and N. Yoshida (2013), Distribution of nitrous oxide dissolved in water masses in the eastern subtropical North Pacific and its origin inferred from isotopomer analysis, *J. Oceanogr.*, *69*, 147–157, doi:10.1007/s10872-012-0162-4.

Füssel, J., P. Lam, G. Lavik, M. M. Jensen, M. Holtappels, M. Gunter, and M. M. Kuypers (2012), Nitrite oxidation in the Namibian oxygen minimum zone, *ISME J.*, *6*, 1200–1209.
Goldhammer, T., V. Brüchert, T. G. Ferdelman, and M. Zabel (2010), Microbial sequestration of phosphorus in anoxic upwelling sediments, *Nat. Geosci.*, *3*, 557–561, doi:10.1038/ngeo913.
Gordon, A. L., and K. T. Bosley (1991), Cyclonic gyre in the tropical South Atlantic, *Deep Sea Res.*, *38*(Suppl. 1), S323–S343.
Goreau, T. J., W. A. Kaplan, S. C. Wofsy, M. B. McElroy, F. W. Valois, and S. W. Watson (1980), Production of NO_{2-} and N_2O by nitrifying bacteria at reduced concentrations of oxygen, *Appl. Environ. Microbiol.*, *40*(3), 526–532.
Granger, J., D. M. Sigman, M. G. Prokopenko, M. F. Lehmann, and P. D. Tortell (2006), A method of nitrite removal in nitrate N and O isotope analyses, *Limnol. Oceanogr. Methods*, *4*, 205–212.
Granger, J., D. M. Sigman, M. F. Lehmann, and P. D. Tortell (2008), Nitrogen and oxygen isotope fractionation during dissimilatory nitrate reduction by denitrifying bacteria, *Limnol. Oceanogr.*, *53*(6), 2533–2545, doi:10.4319/lo.2008.53.6.2533.
Gruber, N., and J. L. Sarmiento (1997), Global patterns of marine nitrogen fixation and denitrification, *Global Biogeochem. Cycles*, *11*(2), 235–266, doi:10.1029/97GB00077.
Gutknecht, E., et al. (2013a), Coupled physical/biogeochemical modeling including O_2-dependent processes in the Eastern Boundary Upwelling Systems: Application in the Benguela, *Biogeosciences*, *10*(6), 3559–3591, doi:10.5194/bg-10-3559-2013.
Gutknecht, E., et al. (2013b), Nitrogen transfers off Walvis Bay: A 3-D coupled physical/biogeochemical modeling approach in the Namibian upwelling system, *Biogeosciences*, *10*(6), 4117–4135, doi:10.5194/bg-10-4117-2013.
Hirsch, A. I., A. M. Michalak, L. M. Bruhwiler, W. Peters, E. J. Dlugokencky, and P. P. Tans (2006), Inverse modeling estimates of the global nitrous oxide surface flux from 1998–2001, *Global Biogeochem. Cycles*, *20*, GB1008, doi:10.1029/2004GB002443.
Hochstein, L. I., M. Betlach, and G. Kritikos (1984), The effect of oxygen on denitrification during steady-state growth of *Paracoccus halodenitrificans*, *Arch. Microbiol.*, *137*, 74–78.
Holland, E. A., J. Lee-Taylor, C. Nevison, and J. Sulzman (2005), Global N cycle: Fluxes and N_2O mixing ratios originating from human activity, doi:10.3334/ORNLDAAC/797.
Hooper, A. B., and K. R. Terry (1979), Hydroxylamine oxidoreductase of *Nitrosomonas* production of nitric oxide from hydroxylamine, *Biochim. Biophys. Acta*, *571*, 12–20.
Houghton, J. T., G. J. Jenkins, and J. J. Ephraums (1991), *Climate change: The IPCC Scientific Assessment*, Cambridge Univ. Press, Cambridge, U. K.
Hutchings, L., et al. (2009), The Benguela Current: An ecosystem of four components, *Prog. Oceanogr.*, *83*(1-4), 15–32, doi:10.1016/j.pocean.2009.07.046.
Jaccard, S. L., and E. D. Galbraith (2011), Large climate-driven changes of oceanic oxygen concentrations during the last deglaciation, *Nat. Geosci.*, *5*(2), 151–156, doi:10.1038/ngeo1352.
Jinuntuya-Nortman, M., R. L. Sutka, P. H. Ostrom, H. Gandhi, and N. E. Ostrom (2008), Isotopologue fractionation during microbial reduction of N_2O within mesocosms as a function of water-filled pore space, *Soil Biol. Biochem.*, *40*, 2273–2280.
Keeling, R. F., A. Körtzinger, and N. Gruber (2010), Ocean deoxygenation in a warming world, *Annu. Rev. Mar. Sci.*, *2*(1), 199–229, doi:10.1146/annurev.marine.010908.163855.
Kim, K.-R., and H. Craig (1990), Two-isotope characterization of N_2O in the Pacific Ocean and constraints on its origin in deep water, *Nature*, *347*, 58–61.
Kritee, K., D. M. Sigman, J. Granger, B. B. Ward, A. Jayakumar, and C. Deutsch (2012), Reduced isotope fractionation by denitrification under conditions relevant to the ocean, *Geochim. Cosmochim. Acta*, *92*, 243–259, doi:10.1016/j.gca.2012.05.020.
Lam, P. J., and J. K. B. Bishop (2008), The continental margin is a key source of iron to the HNLC North Pacific Ocean, *Geophys. Res. Lett.*, *35*, L07608, doi:10.1029/2008GL033294.
Large, W. G., J. C. McWilliams, and S. C. Doney (1994), Oceanic vertical mixing: A review and a model with a nonlocal boundary layer parameterization, *Rev. Geophys.*, *32*(4), 363–403, doi:10.1029/94RG01872.
Law, C. S., and N. J. P. Owens (1990), Significant flux of atmospheric nitrous oxide from the northwest Indian Ocean, *Nature*, *346*, 826–828.
Lehmann, M. F., D. M. Sigman, and W. M. Berelson (2004), Coupling the $^{15}N/^{14}N$ and $^{18}O/^{16}O$ of nitrate as a constraint on benthic nitrogen cycling, *Mar. Chem.*, *88*, 1–20.
Lehmann, M. F., D. M. Sigman, D. C. McCorkle, J. Granger, S. Hoffman, G. Cane, B. G. Brunelle (2007), The distribution of nitrate $^{15}N/^{14}N$ in marine sediments and the impact of benthic nitrogen loss on the isotopic composition of oceanic nitrate, *Geochim. Cosmochim. Acta*, *71*, 5384–5404.
Löscher, C. R., A. Kock, M. Könneke, J. LaRoche, H. W. Bange, and R. A. Schmitz (2012), Production of oceanic nitrous oxide by ammonia-oxidizing archaea, *Biogeosciences*, *9*(7), 2419–2429, doi:10.5194/bg-9-2419-2012.
Lueker, T. J., S. J. Walker, M. K. Vollmer, R. K. Keeling, C. D. Nevison, and R. F. Weiss (2003), Coastal upwelling air-sea fluxes revealed in atmospheric observations of O_2/N_2, CO_2 and N_2O, *Geophys. Res. Lett.*, *30*(6), 1292, doi:10.1029/2002GL016615.
Machida, T., T. Nakazawa, Y. Fujii, S. Aoki, and O. Watanabe (1995), Increase in the atmospheric nitrous oxide concentration during the last 250 years, *Geophys. Res. Lett.*, *22*(21), 2921–2924, doi:10.1029/95GL02822.
Marshall, J., and K. Speer (2012), Closure of the meridional overturning circulation through Southern Ocean upwelling, *Nat. Geosci.*, *5*(3), 171–180, doi:10.1038/ngeo1391.
McIlvin, M. R., and K. L. Casciotti (2010), Automated stable isotopic analysis of dissolved nitrous oxide at natural abundance levels, *Limnol. Oceanogr. Methods*, *8*, 54–66.
McKenney, D. J., C. F. Drury, W. I. Findlay, B. Mutus, T. McDonnell, and C. Gajda (1994), Kinetics of denitrification by *Pseudomonas fluorescens*: Oxygen effects, *Soil Biol. Biochem.*, *26*(7), 901–908.
Menyailo, O. V., and B. A. Hungate (2006), Stable isotope discrimination during soil denitrification: Production and consumption of nitrous oxide, *Global Biogeochem. Cycles*, *20*, GB3025, doi:10.1029/2005GB002527.
Milliff, R. F., and J. Morzel (2001), The global distribution of the time-average wind stress curl from NSCAT, *J. Atmos. Sci.*, *58*(2), 109–131, doi:10.1175/1520-0469(2001)058 < 0109:TGDOTT > 2.0.CO;2.
Naqvi, S. W. A., T. Yoshinari, D. A. Jayakumar, M. A. Altabet, P. V. Narvekar, A. H. Devol, J. A. Brandes, and L. A. Codispoti (1998), Budgetary and biogeochemical implications of N_2O isotope signatures in the Arabian Sea, *Nature*, *394*, 462–465.
Nevison, C., and E. Holland (1997), A reexamination of the impact of anthropogenically fixed nitrogen on atmospheric N_2O and the stratospheric O_3 layer, *J. Geophys. Res.*, *102*(D21), 25,519–25,536, doi:10.1029/97JD02391.
Nevison, C., J. H. Butler, and J. W. Elkins (2003), Global distribution of N_2O and the ΔN_2O-AOU yield in the subsurface ocean, *Global Biogeochem. Cycles*, *17*(4), 1119, doi:10.1029/2003GB002068.
Nevison, C. D., R. F. Weiss, and D. J. Erickson (1995), Global oceanic emissions of nitrous oxide, *J. Geophys. Res.*, *100*(C8), 15,809–15,820, doi:10.1029/95JC00684.

Nevison, C. D., T. J. Lueker, and R. F. Weiss (2004), Quantifying the nitrous oxide source from coastal upwelling, *Global Biogeochem. Cycles*, *18*, GB1018, doi:10.1029/2003GB002110.
Noble, A. E., et al. (2012), Basin-scale inputs of cobalt, iron, and manganese from the Benguela-Angola front into the South Atlantic Ocean, *Limnol. Oceanogr.*, *57*(4), 989–1010.
Ostrom, N. E., M. E. Russ, B. Popp, T. M. Rust, and D. M. Karl (2000), Mechanisms of nitrous oxide production in the subtropical North Pacific based on determinations of the isotopic abundances of nitrous oxide and di-oxygen, *Chemosphere-Global Change Sci.*, *2*, 281–290.
Ostrom, N. E., A. Pitt, P. H. Ostrom, A. S. Grandy, K. M. Huizinga, and G. P. Robertson (2007), Isotopologue effects during N_2O reduction in soils and in pure cultures of denitrifiers, *J. Geophys. Res.*, *112*, G02005, doi:10.1029/2006JG000287.
Ostrom, N. E., H. Gandhi, B. Kamphuis, S. DeCamp, Z. Liu, M. J. McCarthy, and W. S. Gardner (2014), Oxygen metabolism and water mass mixing in the northern Gulf of Mexico hypoxic zone in 2010, *Geochim. Cosmochim. Acta*, *140*, 39–49.
Park, S., et al. (2012), Trends and seasonal cycles in the isotopic composition of nitrous oxide since 1940, *Nat. Geosci.*, *5*(4), 261–265, doi:10.1038/ngeo1421.
Poisson, A., and C. A. Chen (1987), Why is there little anthropogenic CO_2 in the Antarctic Bottom Water?, *Deep Sea Res.*, *34*(7), 1255–1275.
Popp, B. N., et al. (2002), Nitrogen and oxygen isotopomeric constraints on the origins and sea-to-air flux of N_2O in the oligotrophic subtropical North Pacific Gyre, *Global Biogeochem. Cycles*, *16*(4), 1064, doi:10.1029/2001GB001806.
Poth, M., and D. Focht (1985), ^{15}N kinetic analysis of N_2O production by *Nitrosomonas europaea*: An examination of nitrifier denitrification, *Appl. Environ. Microbiol.*, *49*(5), 1134–1141.
Prather, M. J. (1998), Time scales in atmospheric chemistry: Coupled perturbations to N_2O, NOy, and O_3, *Science*, *279*(5355), 1339–1341, doi:10.1126/science.279.5355.1339.
Reuer, M. K., B. A. Barnett, M. L. Bender, P. G. Falkowski, and M. B. Hendricks (2007), New estimates of Southern Ocean biological production rates from O_2/Ar ratios and the triple isotope composition of O_2, *Deep Sea Res., Part I*, *54*(6), 951–974, doi:10.1016/j.dsr.2007.02.007.
Ritchie, G. A. F., and D. J. D. Nicholas (1972), Identification of the sources of nitrous oxide produced by oxidative and reductive processes in *Nitrosomonas europaea*, *Atmos. Sci. J.*, *126*, 1181–1191.
Santoro, A. E., K. L. Casciotti, and C. A. Francis (2010), Activity, abundance and diversity of nitrifying archaea and bacteria in the central California Current, *Environ. Microbiol.*, *12*, 1989–2006, doi:10.1111/j.1462-2920.2010.02205.x.
Santoro, A. E., C. Buchwald, M. R. McIlvin, and K. L. Casciotti (2011), Isotopic signatures of N_2O produced by marine ammonia-oxidizing archaea, *Science*, *333*(6047), 1282–5, doi:10.1126/science.1208239.
Sarmiento, J. L., N. Gruber, M. A. Brzezinski, and J. P. Dunne (2004), High-latitude controls of thermocline nutrients and low latitude biological productivity, *Nature*, *427*, 57–60.
Sasaki, Y., et al. (2011), Biogeochemistry of nitrous oxide in Lake Kizaki, Japan, elucidated by nitrous oxide isotopomer analysis, *J. Geophys. Res.*, *116*, G04030, doi:10.1029/2010JG001589.
Schmidt, H.-L., R. A. Werner, N. Yoshida, and R. Well (2004), Is the isotopic composition of nitrous oxide an indicator for its origin from nitrification or denitrification? A theoretical approach from referred data and microbiological and enzyme kinetic aspects, *Rapid Commun. Mass Spectrom.*, *18*, 2036–2040.
Schmittner, A., and E. D. Galbraith (2008), Glacial greenhouse-gas fluctuations controlled by ocean circulation changes, *Nature*, *456*, 373–376.
Sohm, J., J. Hilton, A. Noble, J. Zehr, M. Saito, and E. Webb (2011), Nitrogen fixation in the South Atlantic Gyre and the Benguela Upwelling System, *Geophys. Res. Lett.*, *38*, L16608, doi:10.1029/2011GL048315.
Sowers, T., R. B. Alley, and J. Jubenville (2003), Ice core records of atmospheric N_2O covering the last 106,000 years, *Science*, *301*, 945–948, doi:10.1126/science.1085293.
Stramma, L., G. C. Johnson, J. Sprintall, and V. Mohrholz (2008), Expanding oxygen-minimum zones in the tropical oceans, *Science*, *320*, 655–658.
Sutka, R. L., N. E. Ostrom, P. H. Ostrom, J. A. Breznak, H. Gandhi, A. J. Pitt, and F. Li (2006), Distinguishing nitrous oxide production from nitrification and denitrification on the basis of isotopomer abundances, *Appl. Environ. Microbiol.*, *72*(1), 638–644.
Sverdrup, H. U., M. W. Johnson, and R. H. Fleming (1942), *The Oceans, Their Physics, Chemistry, and General Biology*, Prentice-Hall, New York.
Toyoda, S., N. Yoshida, T. Miwa, Y. Matsui, H. Yamagishi, and U. Tsunogai (2002), Production mechanism and global budget of N_2O inferred from its isotopomers in the western North Pacific. *Geophys. Res. Lett.*, *29*(3), 7174, doi:10.1029/2001GL014311.
Toyoda, S., H. Mutobe, H. Yamagishi, N. Yoshida, and Y. Tanji (2005), Fractionation of N_2O isotopomers during production by denitrifier, *Soil Biol. Biochem.*, *37*, 1535–1545.
Tsuchiya, M., L. D. Talley, and M. S. McCartney (1994), Water-mass distributions in the western South Atlantic: A section from South Georgia Island (54°S) northward across the equator, *J. Mar. Res.*, *52*, 55–81.
Versteeg, G. F., and W. P. M. Van Swaaij (1988), Solubility and diffusivity of acid gases (CO_2, N_2O) in aqueous alkenolamine solutions, *J. Chem. Eng. Data*, *33*(1), 29–34.
Wanninkhof, R. (1992), Relationship between wind speed and gas exchange over the ocean, *J. Geophys. Res.*, *97*(C5), 7373–7382, doi:10.1029/92JC00188.
Ward, B. B., R. J. Olson, and M. J. Perry (1982), Microbial nitrification rates in the primary nitrite maximum off Southern California, *Deep Sea Res.*, *29*(2A), 247–255.
Weiss, R. F., and B. A. Price (1980), Nitrous oxide solubility in water and seawater, *Mar. Chem.*, *8*(4), 347–359, doi:10.1016/0304-4203(80)90024-9.
Westley, M. B., H. Yamagishi, B. N. Popp, and N. Yoshida (2006), Nitrous oxide cycling in the Black Sea inferred from stable isotope and isotopomer distributions, *Deep Sea Res., Part II*, *53*, 1802–1816.
Yamagishi, H., M. B. Westley, B. Popp, S. Toyoda, N. Yoshida, S. Watanabe, and K. Koba (2007), Role of nitrification and denitrification on the nitrous oxide cycle in the eastern tropical North Pacific and Gulf of California, *J. Geophys. Res.*, *112*, G02015, doi:10.1029/2006JG000227.
Yoshida, N., and S. Toyoda (2000), Constraining the atmospheric N_2O budget from intramolecular site preference in N_2O isotopomers, *Nature*, *405*, 330–334.
Yoshida, N., et al. (1989), Nitrification rates and ^{15}N abundances of N_2O and NO_3^- in the western North Pacific, *Nature*, *342*, 895–897.
Yoshinari, T. (1976), Nitrous oxide in the sea, *Mar. Chem.*, *4*, 189–202.
Yoshinari, T., M. A. Altabet, S. W. A. Naqvi, L. Codispoti, A. Jayakumar, M. Kuhland, and A. Devol (1997), Nitrogen and oxygen isotopic composition of N_2O from suboxic waters of the eastern tropical North Pacific and the Arabian Sea—Measurement by continuous-flow isotope-ratio monitoring, *Mar. Chem.*, *56*, 253–264.
Zamora, L. M., A. Oschlies, H. W. Bange, K. B. Huebert, J. D. Craig, A. Kock, and C. R. Löscher (2012), Nitrous oxide dynamics in low oxygen regions of the Pacific: Insights from the MEMENTO database, *Biogeosciences*, *9*(12), 5007–5022, doi:10.5194/bg-9-5007-2012.